

Article

Highly Active TiO₂ Microspheres Formation in the Presence of Ethylammonium Nitrate Ionic Liquid

Anna Gołabiewska ¹, Micaela Checa-Suárez ^{1,2}, Marta Paszkiewicz-Gawron ¹,
Wojciech Lisowski ³ , Edyta Raczuk ¹, Tomasz Klimczuk ⁴, Żaneta Polkowska ⁵,
Ewelina Grabowska ¹, Adriana Zaleska-Medynska ¹  and Justyna Łuczak ^{6,*}

¹ Faculty of Chemistry, University of Gdansk, 80-308 Gdansk, Poland; anna.golabiewska@ug.edu.pl (A.G.); micaela.checa@epn.edu.ec (M.C.-S.); marta.paszkiewicz@phdstud.ug.edu.pl (M.P.-G.); edyta.raczuk@gmail.com (E.R.); ewelina.grabowska@ug.edu.pl (E.G.); adriana.zaleska@ug.edu.pl (A.Z.-M.)

² Faculty of Civil and Environmental Engineering, Escuela Politécnica Nacional, Quito 170525, Ecuador

³ Institute of Physical Chemistry, Polish Academy of Sciences, 01-224 Warsaw, Poland; wlisowski@ichf.edu.pl

⁴ Faculty of Applied Physics and Mathematics, Gdansk University of Technology, 80-233 Gdansk, Poland; t.klimczuk@gmail.com

⁵ Department of Analytical Chemistry, Faculty of Chemistry, Gdansk University of Technology, 80-233 Gdańsk, Poland; zanpolko@pg.gda.pl

⁶ Department of Chemical Technology, Faculty of Chemistry, Gdansk University of Technology, 80-233 Gdansk, Poland

* Correspondence: justyna.luczak@pg.gda.pl; Tel.: +48-58-347-13-65

Received: 14 May 2018; Accepted: 13 June 2018; Published: 11 July 2018



Abstract: Spherical microparticles of TiO₂ were synthesized by the ionic liquid-assisted solvothermal method at different reaction times (3, 6, 12, and 24 h). The properties of the prepared photocatalysts were investigated by means of UV-VIS diffuse-reflectance spectroscopy (DRS), Brunauer–Emmett–Teller (BET) surface area measurements, scanning electron microscopy (SEM), X-ray diffraction analysis (XRD), and X-ray photoelectron spectroscopy (XPS). The results indicated that the efficiency of the phenol degradation was related to the time of the solvothermal synthesis, as determined for the TiO₂_EAN(1:1)_24h sample. The microparticles of TiO₂_EAN(1:1)_3h that formed during only 3 h of the synthesis time revealed a really high photoactivity under visible irradiation (75%). This value increased to 80% and 82% after 12 h and 24 h, respectively. The photoactivity increase was accompanied by the increase of the specific surface area, thus the poresize as well as the ability to absorb UV-VIS irradiation. The high efficiency of the phenol degradation of the ionic liquid (IL)–TiO₂ photocatalysts was ascribed to the interaction between the surface of the TiO₂ and ionic liquid components (carbon and nitrogen).

Keywords: ionic liquids; ionic liquid-assisted solvothermal reaction; reaction time; titanium dioxide; heterogeneous photocatalysis; visible light

1. Introduction

A number of recent studies have explored the applications of photosensitized titanium dioxide photocatalysts inter alia in solar cells, energy storage, hydrogen production via the water-splitting process, and the photocatalytic degradation of organic pollutants for water/air purification [1–5]. Expected low exploitation costs, prevalence in utility, and safety has created the motivation for intensified research in the field of solar to chemical energy conversion. The photoactive performance of the pristine TiO₂ nano- and micro-particles is limited by its 3.2 eV bandgap to the absorption of UV light. As the UV light range constitutes the total radiant energy in only as diminutive an amount as 5%, harvesting a greater range of the solar spectrum is considered vital for achieving the significant

effectiveness of the photocatalysis [5,6]. The extension of the TiO₂ spectral response range to absorb the photons under visible (43%) or/and near infrared (49% of solar spectrum energy) irradiation is crucial for this purpose. The TiO₂ photocatalytic properties can be controlled and their optical response can be expanded to absorb photons under visible or/and near infrared light irradiation through the alteration of the TiO₂ bandgap via morphology engineering [7–10].

It was found that, after excitation, the electrons and holes propagate to the nano- and micro-particles surface where they react with electron acceptors and donors, respectively [6,9,11,12]. Additionally, it has been noted that a slower recombination rate and a larger surface area accounted for more active adsorption/desorption reactions and the surface transfer of photoexcited electrons [9,12,13], whereas the potential adverse effects that originate in the highly defective sites, typically developing with the growth of a large surface area, may be rectified by a higher crystallization of the particles [9].

Ionic liquids (ILs) have gained increasing attention in terms of their assistance in TiO₂ synthesis as solvents as well as spatial and, perhaps, band structuring agents. Their high viscosity, dielectric constant, and thus polarity and dispersal capacity are widely recognized as the properties responsible for the charge, steric, and viscous stabilization of small-sized slow-growing crystallites, as well as the hindrance of aggregation and agglomeration processes that are disadvantageous for photocatalytic [7,10,11,14–23].

The synthesized photocatalysts in the presence of ILs nano- and microparticles are characterized by a larger specific surface area, higher crystallization level, and less crystalline defects [17]. Hence, with the assistance of ILs, the formation of the particles of the beneficial surface reactivity is promoted, inducing a more effective photon absorption, trapping, and their migration to the surface. Moreover, an energetically simplified pathway of excited electrons through an ionic liquid's HOMO and LUMO orbitals [16], along with prolonged stabilized charge separation was revealed to result in the formation of a greater amount of reactive oxygen species (ROS) in the subsequent reaction of electrons and holes with oxygen and water, respectively. The generated reactive oxygen species ($\bullet\text{OH}$ and $\text{O}_2\bullet^-$) are crucial reagents in the photodegradation of pollutants [16,17,24].

Notwithstanding, the direct relationship between the structure of the ILs and the size/morphology of the nano- and microparticles of the semiconductors, such as the TiO₂ photocatalysts, still remains ambiguous. Up until now, the following factors had been reported as predominant in effectuating the structure, and thus the activity of said particles, as follows: (1) IL anion type (the number of atoms it is composed of growth; apart from this, π - π stacking of imidazolium cations promotes the ILs role as templating agents); (3) cation-anion interaction energy where the frailer, the weaker the cation-anion interactions, the firmer the capping on growing the TiO₂ particles and the more efficient the inhibition/hampering of the unfavorable Ostwald ripening process; and (4) the type of overall interactions (π - π , van der Waals, coulomb and electrostatic forces, and hydrogen bonding) [15,16,21,25].

Furthermore, the proposed *fons et origo* of the influences on the TiO₂ photoactivity are tenable, as follows: (1) doping with N, C, and F elements after ILs thermal decomposition; (2) directly sensitizing the TiO₂ particles; (3) affecting the transfer of photo-generated charges through the bulk of particles; and (4) favoring oxygen vacancies and Ti³⁺ species formation during synthesis [26–28]. However, an up to date kinetics of the formation of the TiO₂ particles during ionic liquid-assisted synthesis has not been presented and discussed.

In this regard, in this study, the TiO₂ particles were synthesized solvothermally, with the assistance of the selected ionic liquid, ethylammonium nitrate [EAN][NO₃], which is one of the earliest reported in the literature of protic ionic liquid [29,30].

Apart from prevailing in studies on the topics of the synthesis process and characterization of the IL-assisted TiO₂ microparticles [22,30–32], we focused on evaluating the functional properties of the obtained micro-particles, namely, their photoactivity. Alongside this, we strived to infer the

mechanisms of the ILs assistance through exploring the influence of selected ILs, illustrated with the example of ethylammonium nitrate [EAN][NO₃] [29].

We placed an emphasis on the essentiality of (1) researching VIS-light induced photoactivity in comparison to the already researched UV-induced photoactivity [19,25,33–35]; and (2) conducting research in the presence of a model pollutant (2a), neutral in terms of the photosensitization of TiO₂, (2b) proposing a simple mechanism of degradation and mineralization, and (2c) with a low photoabsorption coefficient [27,36,37]. In contrast to the common choice of organic dyes (methylene blue, methyl orange, and rhodamine B) [7,10,13,18,19,25,38,39], we applied phenol. Another imperative was that we excluded the minor ones in facilitating the photocatalysis reaction active species, while exposing the substantial ones through the active species scavenger tests.

In this article, we present the results of the previously non-analyzed and non-reviewed comprehensively [EAN][NO₃]-assisted TiO₂ microparticles, where the photocatalytic effect on the degradation and mineralization of phenol in aqueous solution vastly exceeded our expectations, reaching as high as an 82% degradation rate in our tests, which are described below. Moreover, for the first time, we have examined the kinetics of the TiO₂ microsphere formation in the presence of ethylammonium nitrite ionic liquid.

2. Results

First of all, a set of samples with selected IL to titanium (IV) butoxide (TBOT) molar ratios were synthesized and characterized, taking into account the surface area and photoactivity. The sample labeling and the amount of ILs to the precursor used during the preparation procedure, as well as the specific surface area, pore volume of the obtained photocatalysts, and their photocatalytic activity under VIS irradiation are given in Table 1. On the basis of the photocatalytic effect, we chose the sample with the highest activity in order to examine the kinetics of the TiO₂ microsphere formation in the presence of ethylammonium nitrite ionic liquid, which is shown in Figure 1. As presented in Table 1, the effect of the solvothermal synthesis duration (3, 6, 12, and 24 h) on the surface properties as well as the photoactivity for the IL:TBOT ratio equaled to 1:1 were also investigated.

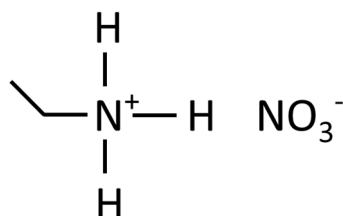


Figure 1. The structure of ethylammonium nitrite [EAN][NO₃] ionic liquid (IL).

2.1. The BET Surface Area and SEM Analysis

The results listed in Table 1 revealed the influence of the ionic liquid content on the specific surface area and the pore volume of the synthesized samples. All of the samples presented a higher specific surface area in comparison with the TiO₂ synthesized without IL (184 m²·g⁻¹), and also than that reported for the commercially available P25 (50 m²·g⁻¹) [10,40]. The values of the specific surface area for TiO₂ prepared in the presence of [EAN][NO₃] ranged from 190 m²·g⁻¹ (sample prepared with the lowest IL:TBOT molar ratio, 1:10) to 233 m²·g⁻¹ for the sample obtained with IL:TBOT, with a molar ratio of 1:2. In this regard, the direct relation between the amount of the IL in the reaction mixture and the specific surface area for these photocatalysts was detected. However, a further increase in the IL content taken for the synthesis (up to IL:TBOT molar ratio of 1:1) resulted in a decrease of the pore volume, thus, the specific surface area was due, most probably, to the overloading of the TiO₂ surface with organic salt. This might indicate that the ILs work like a designer agent of the microstructures' physical and structural properties.

The scanning electron microscopy images of the pure TiO₂ and IL-assisted TiO₂ particles obtained for various molar ratios of IL:TBOT in the presence of [EAN][NO₃] are presented in Figure 2. The pristine TiO₂ exhibited a smooth surface with an average size from 0.5–4 μm. In the case of the IL–TiO₂ samples, it showed that the sample with the molar ratio 1:1 and the sample with a low amount of IL (1:8) presented a spherical structure and did not change in relation to the pristine TiO₂.

Table 1. Characteristics of the TiO₂ particles obtained by ethylammonium nitrite [EAN][NO₃] assisted solvothermal synthesis. IL—ionic liquid; TBOT—titanium (IV) butoxide.

Sample	Time of the Synthesis	Molar Ratio (IL:TBOT)	Specific Surface Area (m ² ·g ⁻¹)	Pore Volume (cm ³ ·g ⁻¹)	Phenol Degradation Efficiency under 60 min of VIS Irradiation (%)	Rate of Phenol Degradation under Visible Light (λ > 420) [μmol·dm ⁻³ ·min ⁻¹]
TiO ₂ _pristine	24	-	184	0.069	7	0.18
TiO ₂ _EAN(1:10)_24h	24	1:10	190	0.093	28	1.01
TiO ₂ _EAN(1:8)_24h	24	1:8	211	0.102	19	0.55
TiO ₂ _EAN(1:5)_24h	24	1:5	216	0.105	33	1.11
TiO ₂ _EAN(1:3)_24h	24	1:3	216	0.105	36	1.17
TiO ₂ _EAN(1:2)_24h	24	1:2	233	0.113	41	1.32
TiO ₂ _EAN(1:1)_24h	24	1:1	221	0.108	82	3.12
TiO ₂ _EAN(1:1)_3h	3	1:1	239	0.12	75	2.28
TiO ₂ _EAN(1:1)_6h	6	1:1	207	0.101	75	2.38
TiO ₂ _EAN(1:1)_12h	12	1:1	209	0.102	80	2.53

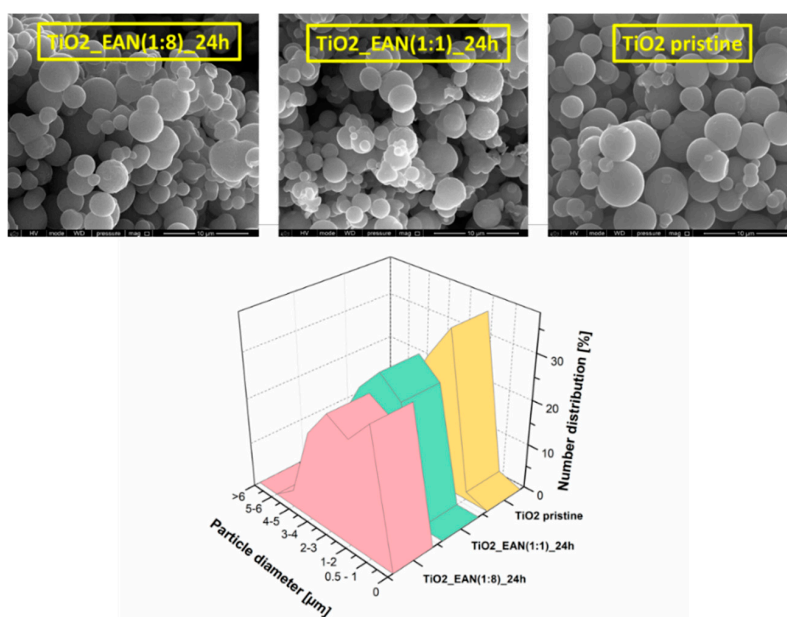


Figure 2. SEM images of TiO₂ obtained from IL-assisted solvothermal synthesis, TiO₂_EAN(1:8)_24h, TiO₂_EAN(1:1)_24h, and reference TiO₂.

The experiments of the TiO₂_EAN(1:1)_24h sample preparation performed at different time regimes revealed that 3 h of solvothermal synthesis was enough to obtain the TiO₂ microspheres (see SEM images, presented in Figure 3 below). However, the reaction yield was relatively low (only 19%) and increased with the increasing reaction time (38% for 6 h, 65% for 12 h, and 93% for 24 h). Moreover, the elongation of the synthesis time resulted, at first, in the decrease of the specific surface area from 239 m²·g⁻¹ (after 3 h) to 207 m²·g⁻¹ (after 6 h), and then in the enlargement of the specific surface area to 221 m²·g⁻¹ (after 24 h).

An explanation of this observation may be found in the SEM images of the microparticles prepared with the same amount of substrates (molar ratio of TBOT to ILs equaling 1:1), however, with different

times of thermal treatment (3, 6, 12, and 24 h) presented in Figure 3. In all of the introduced variations, the majority of the particles lay within the scope of 1–3 μm for 3 h (48%), 2–3 μm for 6 (24%) and 24 h (28%), and 3–4 μm for 12 h (19%). The percentage contribution of the particles with a diameter above 4 μm was rarely reached and never exceeded 15% for all of the obtained samples. In the image sequences presented below, we noted that the sample subjected to thermal treatment for 3 h was mainly composed of a large number of small spherical particles with a range of 1–3 μm . Nonetheless, between the particles synthesized in 6, 12, and 24 h regimes, less of a difference was recognized. In this regard, the high surface area of the particles prepared within 3 h may be related to a higher contribution of the smallest particles.

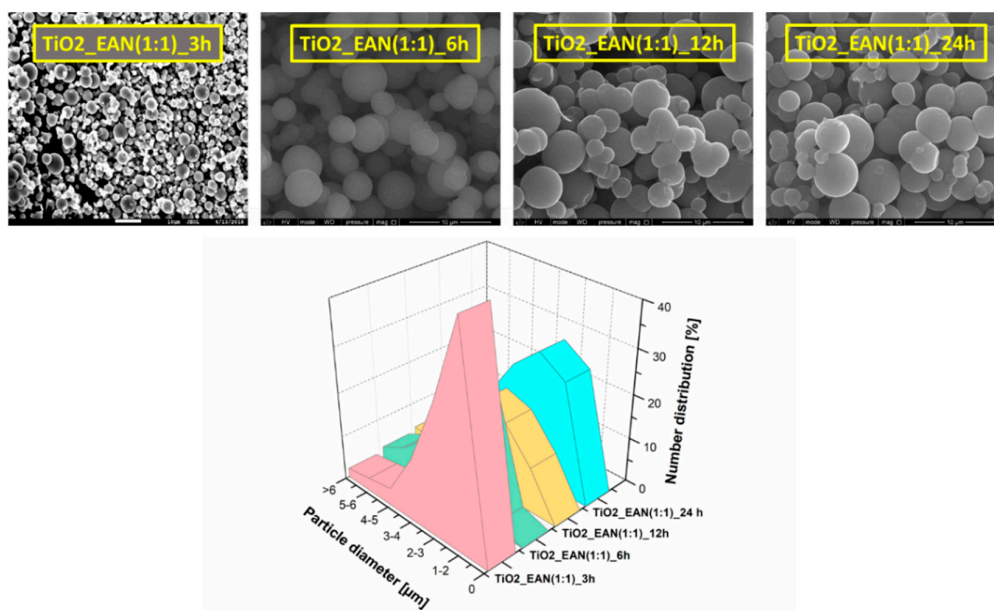


Figure 3. SEM images of $\text{TiO}_2\text{-EAN}(1:1)$ obtained in different synthesis times of 3, 6, 12, and 24 h.

2.2. XRD Analysis

The PXRD patterns for the series of $\text{TiO}_2\text{-EAN}$ are presented in Figures 4 and 5. All of the patterns looked similar as the samples only contained the anatase (TiO_2) phase. The open circles represent the experimental data points, a solid red line is a profile fitting (LeBail method), and the vertical bars mark the positions of the expected Bragg reflections for the used model (I 41/a m d, s.g. #141). The LeBail fit given lattice parameters for TiO_2 are gathered in Table 2. The lattice parameters were similar and are close to those reported by Djerdj and Tonejc [41]. The PXRD reflections were broad, which indicated a small crystallite size estimated to be between 5.0 and 6.5 nm. However, no correlation was observed between the amount of ionic liquid taken for the synthesis nor for the preparation time and the crystallite size.

Table 2. Lattice parameters and average crystallite size of the $\text{TiO}_2\text{-EAN}$ photocatalysts.

Sample	a (Å)	c (Å)	d (Å)
$\text{TiO}_2\text{-EAN}(1:1)\text{-3h}$	3.8051(3)	9.554(2)	65
$\text{TiO}_2\text{-EAN}(1:1)\text{-6h}$	3.7907(7)	9.504(3)	50
$\text{TiO}_2\text{-EAN}(1:1)\text{-12h}$	3.7892(6)	9.507(3)	55
$\text{TiO}_2\text{-EAN}(1:1)\text{-24h}$	3.7890(6)	9.502(3)	60
$\text{TiO}_2\text{-EAN}(1:2)\text{-24h}$	3.7899(7)	9.499(3)	55
$\text{TiO}_2\text{-EAN}(1:3)\text{-24h}$	3.7926(8)	9.506(4)	60
$\text{TiO}_2\text{-EAN}(1:5)\text{-24h}$	3.7814(11)	9.472(6)	65
$\text{TiO}_2\text{-EAN}(1:8)\text{-24h}$	3.7953(9)	9.483(5)	55
$\text{TiO}_2\text{-EAN}(1:10)\text{-24h}$	3.7942(12)	9.476(7)	55

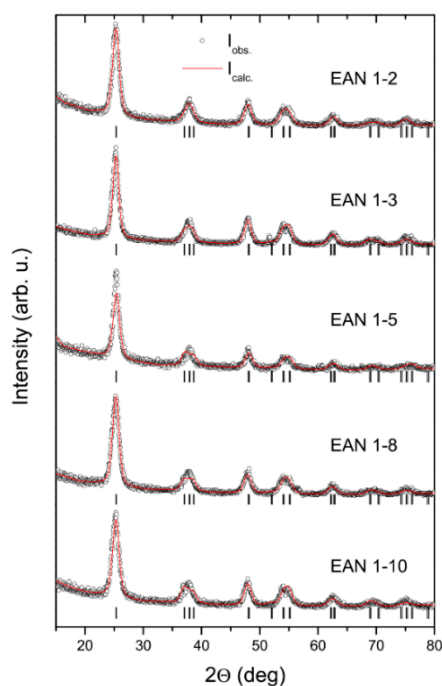


Figure 4. XRD pattern of TiO_2 _EAN prepared with different IL–titanium (IV) butoxide (TBOT) molar ratios. A solid line is a profile fit to the experimental data (open circles). The Bragg reflections are marked by vertical bars.

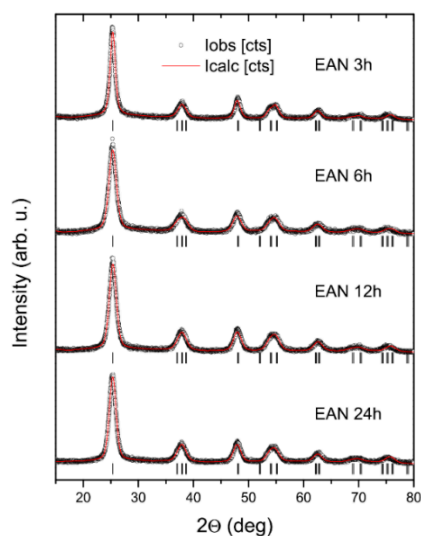


Figure 5. XRD pattern of the TiO_2 _EAN prepared with the IL–TBOT molar ratio of 1:1, synthesized at different synthesis times. A solid line is a profile fit to the experimental data (open circles). The Bragg reflections are marked by vertical bars.

2.3. X-ray Photoelectron Spectroscopy (XPS) Analysis

The elemental surface composition of the selected IL– TiO_2 specimens, evaluated by XPS, is shown in Table 3. Titanium, oxygen, carbon, and nitrogen were detected and the corresponding high-resolution (HR) XPS spectra of Ti 2p, O 1s, C 1s, and N 1s are presented in Figure 6. The chemical character of the elements is identified in the deconvoluted spectra in Figure 6 and Table 3. The Ti 2p, O 1s, and C 1s spectra exhibited features that were characteristic of the IL– TiO_2 specimens [16,42]. The N 1s signal at 400 eV is commonly interpreted as the surface C–N bond. Only for the TiO_2 _EAN(1:1)

sample thermally treated for 24 h was the additional signal that appeared at about 402.8 eV observed, which may be assigned to the oxidized nitrogen surface species.

The XPS data collected in Table 3 revealed that the surface chemical composition of the TiO₂_EAN(1:1)_24h samples were different than the sample of the lower amount of TiO₂_EAN(1:8)_24h. For the last one, the contribution of the Ti⁽³⁺⁾ fraction was about 30% smaller and the nitrogen amount was evidently lower than for the TiO₂_EAN(1:1)_24h sample. These observations confirmed a higher amount of IL on the TiO₂_EAN(1:1)_24h sample surface (an analogous relation was also observed for the carbon atom). In the series of TiO₂_EAN(1:1) samples, differing by the time of thermal treatment, we noted a systematic decrease in the oxygen of the Ti–O_{surf} fraction, with an increasing time of the thermal treatment from 6 to 24 h, and a significantly smaller surface concentration of nitrogen for the 24 h synthesized sample (Table 3). Moreover, for the last sample, the oxidized form of the nitrogen species appeared in addition to the main nitrogen N–C surface fraction (Figure 6). These observations indicated the surface transformation of the IL-assisted TiO₂ with the prolonged time of thermal treatment.

To elucidate the effect of the phenol-degradation processing on the chemical composition of the TiO₂_EAN photocatalyst, we analyzed both the sample after three cycles of photocatalytic processing and the same sample washed with deionized water. The results are compared in Figure 6 and Table 3. One can see that the nitrogen atom concentration was similar for both of the samples. However, the water washed sample exhibited a significantly larger surface amount of titanium fraction Ti⁽³⁺⁾ and a relatively higher contribution of –OH surface species (see O 1s and C 1s fractions in Table 3).

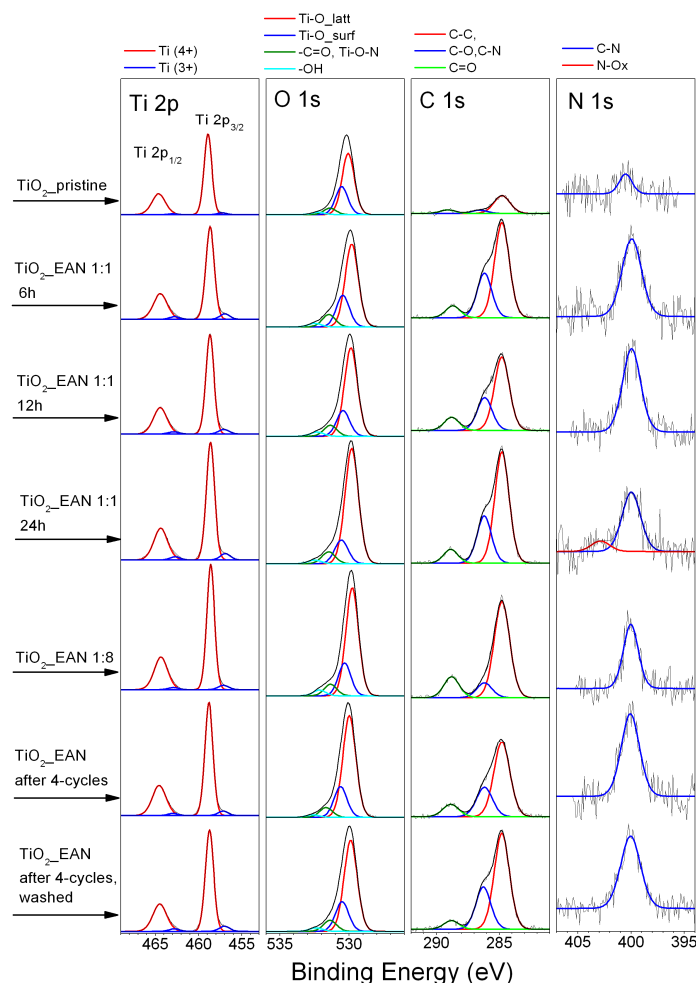


Figure 6. High resolution X-ray photoelectron spectroscopy (XPS) spectra of elements detected in the surface layer of the [EAN][NO₃]-modified TiO₂ particles.

Table 3. Elemental composition (in at. %) and chemical character of titanium, oxygen, carbon, and nitrogen states in the surface layer of [EAN][NO₃]-modified TiO₂ particles, evaluated by X-ray photoelectron spectroscopy (XPS) analysis.

Sample Label	Ti 2p _{3/2} Fraction (%)			Σ O (at. %)	O 1s Fraction (%)				Σ C (at. %)	C 1s Fraction (%)			Σ N (at. %)	N 1s Fraction (%)	
	Σ Ti (at. %)	Ti ⁽⁴⁺⁾ 458.7 ± 0.1 eV	Ti ⁽³⁺⁾ 457.0 ± 0.1 eV		Ti-O _{latt} 529.9 ± 0.1 eV	Ti-O _{surf} 530.5 ± 0.1 eV	-Ti-O-N, -C=O 531.5 ± 0.1 eV	-OH 532.4 ± 0.1 eV		"A" C-C 284.8 eV	"B" C-OH, C-N 286.2 ± 0.1 eV	"C" -C=O, 288.9 ± 0.1 eV		N-C 399.9 ± 0.1 eV	N-O _x 402.8 ± 0.1 eV
TiO ₂ _pristine	29.44	97.59	2.41	66.27	62.35	28.60	6.59	2.46	4.15	72.27	13.46	14.27	0.14	100	0
TiO ₂ _EAN 1:1_6h	23.15	93.37	6.63	61.97	63.55	24.13	9.54	2.78	14.35	63.03	29.19	7.78	0.53	100	0
TiO ₂ _EAN 1:1_12h	24.00	94.06	5.94	63.51	68.33	19.89	8.50	3.28	11.94	61.53	27.49	10.99	0.54	100	0
TiO ₂ _EAN 1:1_24h	23.37	93.64	6.36	63.00	74.56	15.33	7.72	2.39	13.24	64.56	27.42	8.02	0.38	84.89	5.11
TiO ₂ _EAN 1:8_24h	24.32	95.44	4.56	63.80	68.52	20.58	7.25	3.65	11.61	73.05	11.18	15.77	0.29	100	0
TiO ₂ _EAN_4-cycles	24.61	94.47	4.78	63.77	70.46	21.06	6.75	1.73	11.14	64.12	25.22	10.66	0.49	100	0
TiO ₂ _EAN_4-cycles (washed)	23.53	93.10	6.13	62.35	67.42	21.84	8.15	2.59	13.64	65.63	28.52	5.84	0.48	100	0

2.4. UV-VIS Spectrum

The UV-VIS adsorption spectra of the TiO₂ synthesized with various molar ratios of [EAN][NO₃] to TBOT are presented in Figure 7. Pristine TiO₂ was only photoactive under the UV region ($\lambda < 400$ nm). The addition of the ionic liquid to the TiO₂ synthesis environment increased the absorption range of IL-TiO₂, being noticeably photoactive at above 420 nm. The absorption properties of the samples prepared with IL were superior in comparison with the pristine TiO₂ in the visible light range, whereas all of the samples showed a similar UV absorption. Generally, a higher IL amount used for synthesis resulted in the enhancement of the VIS light absorption by the IL-TiO₂ photocatalysts.

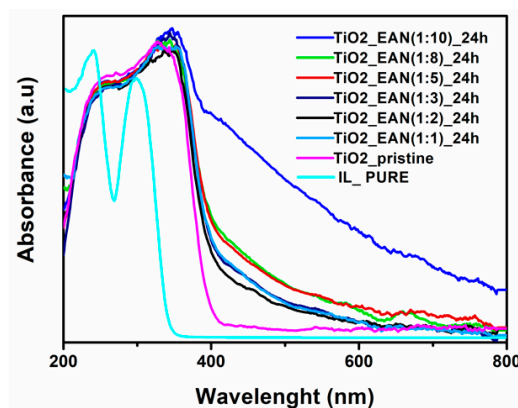


Figure 7. UV-VIS adsorption spectra of TiO₂ synthesized using various molar ratios of [EAN][NO₃] to TBOT.

Interesting results were also obtained for the experiments where the influence of the reaction time was taken into account (Figure 8). When increasing the reaction time, the enhancement of the visible light absorption by IL-TiO₂ was observed. Thereby, the sample prepared during 24 h was characterized by a significantly broader absorption as well as the highest red shift of the absorption edge; thus, there was a higher effectiveness in creating the electron-hole pairs.

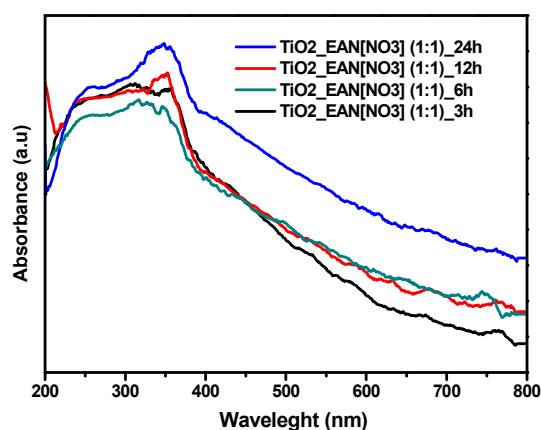


Figure 8. UV-VIS adsorption spectra of TiO₂_EAN(1:1) photocatalyst prepared in 3, 6, 12, and 24 h.

According to the literature, a significant increase in the absorption of visible light by TiO₂ can be related with the presence of carbon atoms in the sample [43–47]. As the carbon species exist mainly on the TiO₂ surface rather than occupying the lattice of TiO₂, the visible light response of the samples was attributed to the formation of the inter band C2p states [48]. However, our observations revealed that a correlation between the content of the IL used for the sample preparation and the apparent enhanced absorption of visible light was not observed. Additionally, based on the XPS analysis, a similar amount

of at. % of carbon was observed for the samples containing small amounts of IL, as well as the sample with a higher IL content.

2.5. Photocatalytic Activity of IL-TiO₂ in Phenol Decomposition Model Reaction

The photocatalytic activity of the IL-TiO₂ samples was evaluated by the degradation of the phenol model compound under visible light ($\lambda > 420$ nm) irradiation. The obtained results are summarized in Table 1 and presented in Figure 9. As above-mentioned, before illumination, the solution was stirred for 30 min in the dark to establish a molecular adsorption equilibrium. Pristine TiO₂ synthesized by the solvothermal method, without addition of the ionic liquid, was used as the reference sample. For comparison purposes, the photocatalytic activity result of P25 TiO₂ under UV-VIS irradiation was also shown.

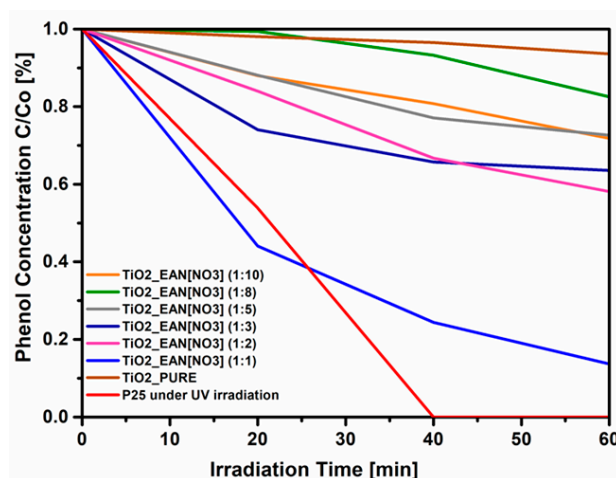


Figure 9. Efficiency of phenol degradation under visible light ($\lambda > 420$ nm) in the presence of TiO₂ prepared in [EAN][NO₃] and under UV-VIS light for P25.

It was found that the TiO₂_EAN microparticles exhibited a higher photoefficiency than the pristine TiO₂, which is also consistent with the higher BET specific surface areas and enhanced optical properties. After 60 min of the photocatalytic process, 7% of the phenol was degraded using unmodified TiO₂, however, the TiO₂_EAN efficiency was higher, and was strongly influenced by the amount of ILs that were used during the synthesis. For example, up to 82% of the phenol was degraded in the presence of photocatalyst TiO₂_EAN(1:1)_24h, where the molar ratio of [EAN][NO₃] to TBOT taken for synthesis was 1:1. This value was about 5.5 times higher when compared to the pristine TiO₂, indicating its excellent photocatalytic activity. This observation was correlated with the UV-VIS adsorption spectra, where the TiO₂_EAN(1:1)_24h sample showed the highest extension of the absorption edge to the visible light region. It was found that the samples prepared with IL:TBOT molar ratios of 1:10 and 1:8 revealed the lowest photoactivity among the photocatalysts that were obtained in the presence of ethylammonium nitrate IL. In this regard, the photodegradation efficiency increased with the increase in the quantity of ionic liquid taken to synthesis (thereby, the IL present at the TiO₂ surface).

In addition, the efficiency of the phenol total mineralization by the sample with the highest photoactivity was also determined. The total organic carbon measurements confirmed 20% of the total mineralization of the phenol after 60 min of irradiation in a presence of the TiO₂_EAN(1:1)_24h sample that was performed under VIS irradiation and 48% under UV-VIS irradiation.

Moreover, the efficiency of the phenol degradation was also related with the time of the solvothermal synthesis, as determined for the TiO₂_EAN(1:1) sample. The microparticles of TiO₂_EAN(1:1)_3h formed during only 3 h of the synthesis time revealed a really high photoactivity under visible irradiation at 75%. This value increased to 80% and 82% after 12 h and 24 h, respectively. The photoactivity increase was accompanied by an increase in the specific surface area, thus the

pore sizes as well as the ability to absorb UV-VIS irradiation. Additionally, based on the XPS measurements, it was concluded that the increase in the visible light absorption and the enhancement of the photocatalytic activity may be related to the highest quantity of the carbon and $\text{Ti}^{(+3)}$ defects at the TiO_2 surface.

To investigate the degradation/regeneration capacity and the structural stability during the entire process, we performed stability tests for the sample characterized by the best photocatalytic activity under VIS light irradiation. In the stability tests, the same sample was repeatedly used in the phenol photodegradation reaction three times. As shown in Figure 10, a significant drop in the phenol removal, from 84% to 33%, was found.

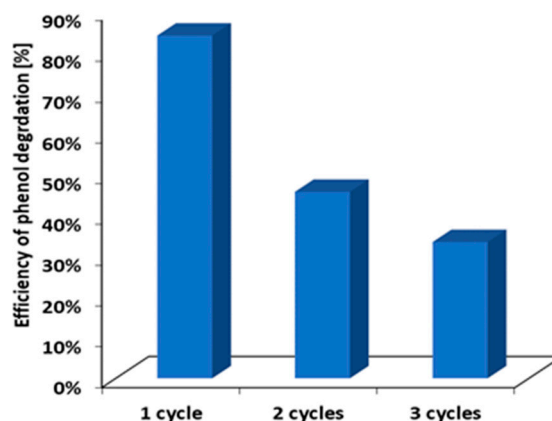


Figure 10. Phenol removals in the photodegradation using the TiO_2 microspheres in a cycled mode.

In order to further clarify the possible mechanism of phenol degradation, reactive species trapping tests were designed. Controlled photoactivity experiments using different radical scavengers (ammonium oxalate as a scavenger for h^+ , AgNO_3 as a scavenger for e^- , benzoquinone as a scavenger for $\text{O}_2\bullet^-$ radical species, and tert-butyl alcohol as a scavenger for $\bullet\text{OH}$ species) were carried out similarly to the above described photocatalytic degradation process. The only exception was that the radical scavengers were added to the reaction system. The addition of ammonium oxalate and AgNO_3 had a weak inhibition efficiency of the phenol degradation, indicating that h^+ and e^- had a negligibly small effect on the mechanism of photocatalytic degradation. The photocatalytic conversion fell by approximately half when the tert-butyl alcohol (TBA) as the scavenger for the hydroxyl radicals was used. As shown in Figure 11, when benzoquinone as the trapping agent of $\text{O}_2\bullet^-$ was added into the phenol solution under visible irradiation, the photodegradation of phenol significantly declined to about 7%. These results clearly suggest that the photocatalytic degradation of phenol under VIS irradiation in the presence of $\text{TiO}_2\text{-EAN}(1:1)$ was mainly intimate, with the photogenerated superoxide radical species. Secondly, the photogenerated OH radicals were also involved in the decomposition of phenol.

To explain what might have contributed to the increase in the photoactivity of $\text{TiO}_2\text{-ILs}$, the decomposition level of the ionic liquid cations was investigated using chromatography techniques. It was demonstrated that the ethylammonium nitrate ionic liquid was degraded in 97% after 24 h of the solvothermal reaction. Therefore, it is most likely that TiO_2 could be doped with nitrogen and carbon, and/or surface-modified by carbon species. However, based on the XPS analysis, the Ti–N interactions between the released nitrogen atoms, resulting from the IL's thermal decomposition, and the TiO_2 matrix, have not been observed. Thus, although we could expect the incorporation of nitrogen and carbon atoms in a crystalline lattice of TiO_2 , the performed analysis did not confirm it. Nevertheless, it should be remembered that because of the low ionic liquid content on the TiO_2 surface, a low level of XPS detection (d.l. = 0.1 at. %) could affect the results. According to the literature, it could be generally stated that if TiO_2 particles grow in the presence of the N and C precursors and under

elevated temperature conditions, usually, the N and C atoms are incorporated into the crystal lattice of the semiconductors [49–51].

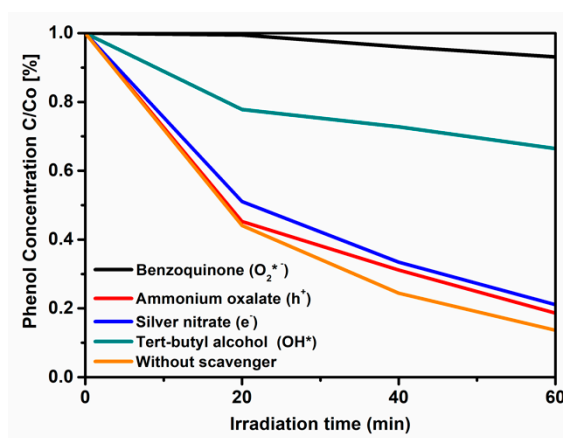


Figure 11. Effect of the addition of different radical scavengers on the phenol degradation over $\text{TiO}_2\text{-EAN}(1:1)\text{-24h}$ composites under visible light irradiation. Initial pH 6.5, 20 mg/L, light intensity 3 mW/cm^2 .

To identify the origin of visible light-induced activity, the phenol degradation rate was plotted depending on the surface area values as well as the carbon and nitrogen content in the surface layer. The data presented in Figure 12 suggests that the observed increase in photoactivity could be most interpreted by the presence of nitrogen in the surface layer. Although the origin of photoactivity is not clear at this moment, it is crucial to note that the preparation of highly active TiO_2 spheres was developed.

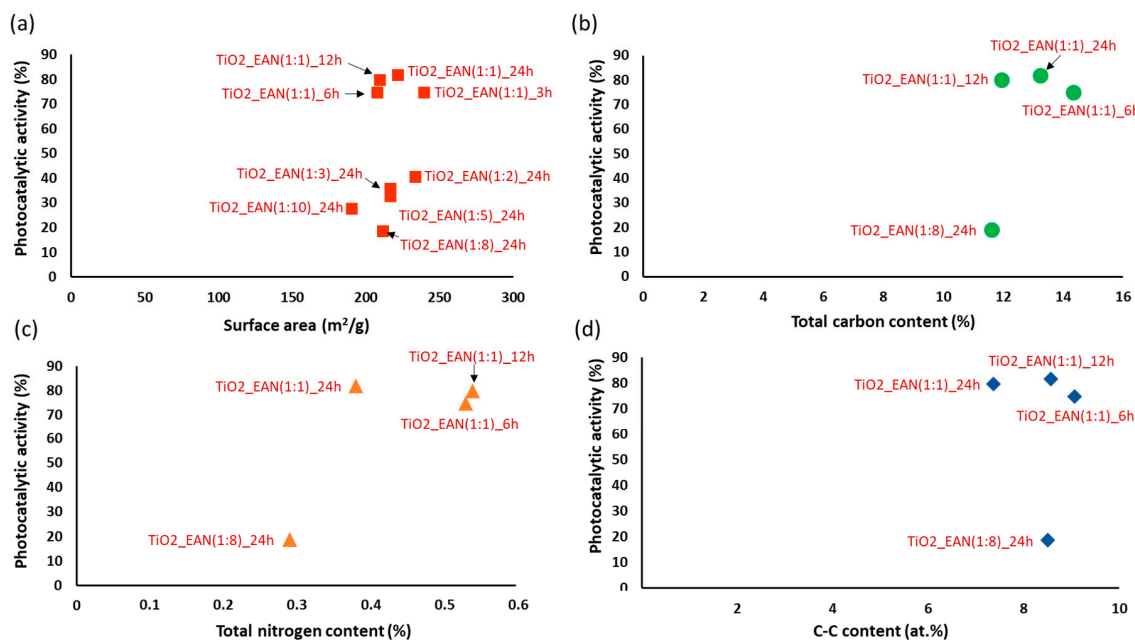


Figure 12. Dependence of the (a) surface area, (b) total carbon content, (c) total nitrogen content (d) C–C content of the photocatalytic activity.

3. Materials and Methods

3.1. Materials

For the aforementioned synthesis' purpose, the following reagents were applied: (1) titanium (IV) butoxide (TBOT) as the TiO₂ micro-particles direct precursor, and (2) 36% hydrochloric acid (HCl) as a pH stabilizer, sourced from Sigma-Aldrich; (3) anhydrous ethyl alcohol (99.8% ethanol) as the reaction medium (from POSCH S.A., Troine, Luxembourg); (4) ethylammonium nitrate (from IOLITEC, Heilbronn, Germany, purveyed with $\geq 97\%$ of purity) as the assisting ionic liquid; and (5) deionized water, provided locally.

3.2. Preparation of IL-Assisted TiO₂ Particles

The preparation of the TiO₂ micro-particles was carried out emulating the method reported by Paszkiewicz et al. [16], summarized as follows: (1) TBOT was dispersed in ethanol through dropwise pouring under constant vigorous stirring; and (2) HCl, deionized water, and the due amount of IL—adequate to the applied molar ratio of TBOT to IL—were dissolved under unchanged conditions, to the point of attaining a pellucid solution. Afterwards, the ensuing mixture was transferred into an inner Teflon and an outer stainless steel autoclave, to be incubated at 180 °C for 24 h (for various TBOT to IL molar ratios) and for 6, 12, and 24 h (for 1:1 TBOT to IL molar ratio) for the purpose of the kinetics of the crystal growth evaluation. Subsequently, the autoclaves were cooled down to room temperature and the obtained precipitate was cleansed through numerous washings with deionized water and ethanol, and then dried at 60 °C for 4 h. The preparation ended with the 2 h calcination of plateau at 200 °C, which was reached at the 2 °C/min slope. For reference, the pristine TiO₂ was as-synthesized, with the exception of the IL presence.

3.3. Surface Properties Characterization

The Brunauer–Emmett–Teller (BET) surface area was calculated by the N₂ absorption–desorption isotherms at 77 K on a Micromeritics Gemini V200 Shimadzu analyzer (equipped with the VacPrep 061 Degasser) (Norcross, GA, USA). The morphology of the TiO₂ micro-particles was studied by scanning electron microscopy (SEM) analysis, performed under a Hitachi TM-1000 microscope (Tokyo, Japan). The chemistry of the surface was researched by X-ray photoelectron spectroscopy (XPS), the results were obtained with a PHI 5000 VersaProbe™ (ULVAC-PHI, Chigasaki, Japan) spectrometer of monochromatic Al K α radiation ($h = 1486.6$ eV). The phase purity of the samples was determined by powder X-ray diffraction (PXRD) using a PANalytical X'Pert Plus diffractometer (Almelo, The Netherlands) with Cu K α radiation. To determine the unit cell parameters, the profile fits were performed on the powder diffraction data through the use of the HighScore program using Thompson–Cox–Hastings pseudo-Voigt peak shapes. The average crystallite size was calculated using the Scherrer equation.

The decomposition level of the ionic liquid cations was analyzed using a Dionex ICS 1100 liquid chromatograph. Deionized water containing 0.21% (v/v) of methanesulfonic acid (Sigma Aldrich, St. Louis, MO, USA) was used as a mobile phase. The separation was carried out isocratically using a Dionex (Sunnyvale, CA, USA) ION PAC, CS16 column (3 \times 250 mm Dionex) at 35 °C. The flow rate was 0.36 mL min⁻¹. Each sample (before and after solvothermal reaction) was measured in triplicate. The decomposition level was calculated as follows:

$$\eta_{\text{IL}}(\%) = 100 \times C_0 - C/C_0$$

where C₀ is the initial concentrations of the cations of the ILs; and C is the concentrations of the cations of the ILs after the solvothermal reaction.

3.4. Evaluation of Photocatalytic Activity

The photocatalytic activity was measured through the phenol decomposition rate under visible-light irradiation. For this aim, we dispersed 0.125 g of the obtained photocatalyst in 25 mL of phenol aqueous solution ($C_0 = 25 \text{ mg/L}$), inside a cylindrical reactor with a circular quartz window. In use, there was a reactor fitted with a cooling jacket; during the reaction, it was cooled by the constant flow of water at $\leq 10 \text{ }^\circ\text{C}$, supplied in aeration at $5 \text{ dm}^3/\text{h}$. The reactor's quartz-windowed side was exposed to the illumination of intensity equaling to 3 mW/cm^2 (by 1000 W Xenon lamp, 6271H Oriol; optical filter $>420 \text{ nm}$, GG 420).

In order to establish the absorption-desorption equilibrium between the phenol and photocatalyst prior to the reaction, the suspension was allocated to 30 min long stirring in the dark, preliminarily to the photo-initiation of the catalysis; then, about 1 mL of the suspension was sampled from the reactor. During the irradiation, the samples were taken in 3 and 20 min intervals. Each sample was filtered through syringe filters ($\Phi = 0.2 \text{ }\mu\text{m}$) for the removal of the photocatalyst micro-particles, anterior to the due evaluation. The concentration of the remaining phenol was measured colorimetrically ($\lambda_{\text{max}} = 480 \text{ nm}$), after the derivatization with diazo-p-nitroaniline with a UV-VIS spectrometer (Evolution 220, Thermo-Scientific, Waltham, MA, USA).

The controlled photoactivity experiments were carried out using different scavengers (ammonium oxalate as a scavenger of photogenerated holes, AgNO_3 for electrons, benzoquinone for superoxide radical species, and tert-butyl alcohol for hydroxyl radical species). The scavenger concentration was equal to the phenol content, and experiments were performed analogously to the photocatalytic degradation of the phenol described in the manuscript, except that the scavengers were added to the reaction system.

4. Conclusions

This study is the first step towards enhancing our understanding of the effect of ethylammonium nitrate ionic liquids on the surface properties of the TiO_2 spheres formed in the solvothermal synthesis. In summary, the TiO_2 microspheres with a superior visible-light photocatalytic activity were prepared in the presence of the ethylammonium nitrate ionic liquid, using a solvothermal method followed by a calcination process. It should be highlighted that the most active TiO_2 samples formed in the presence of $[\text{EAN}][\text{NO}_3]$ possessed almost the same activity induced by visible light than P25 TiO_2 under UV radiation. The phenol degradation rate was equal to $3.12 \text{ }\mu\text{mol/dm}^3/\text{min}$ for the $\text{TiO}_2\text{-EAN/Vis}$ system, and $3.46 \text{ }\mu\text{mol/dm}^3/\text{min}$ for the P25/UV system. In this paper, the kinetics of the highly active TiO_2 microsphere formation in the presence of ethylammonium nitrate ionic liquid was examined. The obtained results revealed that the micro-particles of $\text{TiO}_2\text{-EAN}(1:1)\text{-3h}$ that formed during only 3 h of synthesis time revealed a really high photoactivity under visible irradiation at 75%. This value increased to 80% and 82% after 12 and 24 h, respectively. However, the reaction yield for the 3 h synthesis time was relatively low (only 19%) and significantly increased with the increasing reaction time (38% for 6 h, 65% for 12 h, and 93% for 24 h). The photoactivity increase was accompanied by an increase in the specific surface area, thus the pore sizes as well as the ability to absorb the VIS irradiation.

The effective interactions between the ionic liquid components, mainly carbon, nitrogen, and the micro-particles surface of TiO_2 , were clearly demonstrated by the XPS analysis. This factor could result in excellent visible-light photocatalytic activity for the IL- TiO_2 samples prepared. The radical trapping experiments revealed that $\text{O}_2^{\bullet-}$ and OH^\bullet were the main active species during the degradation process.

Author Contributions: Conceptualization, A.Z.-M. and J.L.; funding acquisition, J.L.; investigation, A.G., M.C.-S., M.P.-G., W.L., E.R., T.K., Ž.P., and J.L.; project administration, E.G.; supervision, A.Z.-M. and J.L.; writing (original draft), A.G., W.L., E.R., T.K., E.G., and J.L.; writing (review and editing), A.Z.-M. and J.L.

Funding: This research was funded by the National Science Center within the program SONATA 8, research grant: 'Influence of the ionic liquid structure on interactions with TiO_2 particles in ionic liquid assisted hydrothermal synthesis', contract No. 2014/15/D/ST5/02747.

Conflicts of Interest: The authors declare no conflict of interest.

References

1. Hoffmann, M.R.; Martin, S.T.; Choi, W.; Bahnemann, D.W. Environmental applications of semiconductor photocatalysis. *Chem. Rev.* **1995**, *95*, 69–96. [[CrossRef](#)]
2. Fujishima, A.; Rao, T.N.; Tryk, D.A. Titanium dioxide photocatalysis. *J. Photochem. Photobiol. C Photochem. Rev.* **2000**, *1*, 1–21. [[CrossRef](#)]
3. Pelaez, M.; Nolan, N.T.; Pillai, S.C.; Seery, M.K.; Falaras, P.; Kontos, A.G.; Dunlop, P.S.M.; Hamilton, J.W.J.; Byrne, J.A.; O'Shea, K.; et al. A review on the visible light active titanium dioxide photocatalysts for environmental applications. *Appl. Catal. B Environ.* **2012**, *125*, 331–349. [[CrossRef](#)]
4. Fox, M.A.; Dulay, M.T. Heterogeneous photocatalysis. *Chem. Rev.* **1993**, *93*, 341–357. [[CrossRef](#)]
5. Thompson, T.L.; Yates, J.T. Surface science studies of the photoactivation of TiO₂ new photochemical processes. *Chem. Rev.* **2006**, *106*, 4428–4453. [[CrossRef](#)] [[PubMed](#)]
6. Zhang, B.; Xue, Z.; Xue, Y.; Huang, Z.; Li, Z.; Hao, J. Ionic liquid-assisted synthesis of morphology-controlled TiO₂ particles with efficient photocatalytic activity. *RSC Adv.* **2015**, *5*, 81108–81114. [[CrossRef](#)]
7. Ramanathan, R.; Bansal, V. Ionic liquid mediated synthesis of nitrogen, carbon and fluorine-codoped rutile TiO₂ nanorods for improved UV and visible light photocatalysis. *RSC Adv.* **2015**, *5*, 1424–1429. [[CrossRef](#)]
8. Xu, H.; Ouyang, S.; Liu, L.; Reunchan, P.; Umezawa, N.; Ye, J. Recent advances in TiO₂-based photocatalysis. *J. Mater. Chem. A* **2014**, *2*, 12642–12661. [[CrossRef](#)]
9. Zhang, F.; Sun, D.; Yu, C.; Yin, Y.; Dai, H.; Shao, G. A sol-gel route to synthesize SiO₂/TiO₂ well-ordered nanocrystalline mesoporous photocatalysts through ionic liquid control. *New J. Chem.* **2015**, *39*, 3065–3070. [[CrossRef](#)]
10. Alammar, T.; Noei, H.; Wang, Y.; Mudring, A.-V. Mild yet phase-selective preparation of TiO₂ nanoparticles from ionic liquids—A critical study. *Nanoscale* **2013**, *5*, 8045–8055. [[CrossRef](#)] [[PubMed](#)]
11. Ahmed, E.; Breternitz, J.; Groh, M.F.; Ruck, M. Ionic liquids as crystallisation media for inorganic materials. *CrystEngComm* **2012**, *14*, 4874–4885. [[CrossRef](#)]
12. Bhattacharyya, K.; Majeed, J.; Dey, K.K.; Ayyub, P.; Tyagi, A.K.; Bharadwaj, S.R. Effect of Mo-Incorporation in the TiO₂ Lattice: A mechanistic basis for photocatalytic dye degradation. *J. Phys. Chem. C* **2014**, *118*, 15946–15962. [[CrossRef](#)]
13. Yu, S.; Liu, B.; Wang, Q.; Gao, Y.; Shi, Y.; Feng, X.; An, X.; Liu, L.; Zhang, J. Ionic Liquid Assisted Chemical Strategy to TiO₂ Hollow Nanocube Assemblies with Surface-Fluorination and Nitridation and High Energy Crystal Facet Exposure for Enhanced Photocatalysis. *ACS Appl. Mater. Interfaces* **2014**, *6*, 10283–10295. [[CrossRef](#)] [[PubMed](#)]
14. Gindri, I.M.; Frizzo, C.P.; Bender, C.R.; Tier, A.Z.; Martins, M.A.P.; Villetti, M.A.; Machado, G.; Rodriguez, L.C.; Rodrigues, D.C. Preparation of TiO₂ nanoparticles coated with ionic liquids: A supramolecular approach. *ACS Appl. Mater. Interfaces* **2014**, *6*, 11536–11543. [[CrossRef](#)] [[PubMed](#)]
15. Łuczak, J.; Paszkiewicz, M.; Krukowska, A.; Malankowska, A.; Zaleska-Medynska, A. Ionic liquids for nano- and microstructures preparation. Part 1: Properties and multifunctional role. *Adv. Colloid Interface Sci.* **2016**, *230*, 13–28. [[CrossRef](#)] [[PubMed](#)]
16. Paszkiewicz, M.; Łuczak, J.; Lisowski, W.; Patyk, P.; Zaleska-Medynska, A. The ILs-assisted solvothermal synthesis of TiO₂ spheres: The effect of ionic liquids on morphology and photoactivity of TiO₂. *Appl. Catal. B Environ.* **2016**, *184*, 223–237. [[CrossRef](#)]
17. Kaur, N.; Singh, V. Current status and future challenges in ionic liquids, functionalized ionic liquids and deep eutectic solvent-mediated synthesis of nanostructured TiO₂: A review. *New J. Chem.* **2017**, *41*, 2844–2868. [[CrossRef](#)]
18. Wender, H.; Feil, A.F.; Diaz, L.B.; Ribeiro, C.S.; Machado, G.J.; Migowski, P.; Weibel, D.E.; Dupont, J.; Teixeira, S.R. Self-organized TiO₂ nanotube arrays: Synthesis by anodization in an ionic liquid and assessment of photocatalytic properties. *ACS Appl. Mater. Interfaces* **2011**, *3*, 1359–1365. [[CrossRef](#)] [[PubMed](#)]
19. Qi, L.; Yu, J.; Jaroniec, M. Enhanced and suppressed effects of ionic liquid on the photocatalytic activity of TiO₂. *Adsorption* **2013**, *19*, 557–561. [[CrossRef](#)]
20. Marr, P.C.; Marr, A.C. Ionic liquid gel materials: Applications in green and sustainable chemistry. *Green Chem.* **2016**, *18*, 105–128. [[CrossRef](#)]

21. Chang, S.-M.; Lee, C.-Y. A salt-assisted approach for the pore-size-tailoring of the ionic-liquid-templated TiO₂ photocatalysts exhibiting high activity. *Appl. Catal. B Environ.* **2013**, *132*, 219–228. [[CrossRef](#)]
22. Lopes, C.W.; Finger, P.H.; Mignoni, M.L.; Emmerich, D.J.; Mendes, F.M.T.; Amorim, S.; Pergher, S.B.C. TiO₂-TON zeolite synthesis using an ionic liquid as a structure-directing agent. *Microporous Mesoporous Mater.* **2015**, *213*, 78–84. [[CrossRef](#)]
23. Yu, N.; Gong, L.; Song, H.; Liu, Y.; Yin, D. Ionic liquid of [Bmim]⁺Cl[−] for the preparation of hierarchical nanostructured rutile titania. *J. Solid State Chem.* **2007**, *180*, 799–803. [[CrossRef](#)]
24. Gołabiewska, A.; Paszkiewicz-Gawron, M.; Sadzińska, A.; Lisowski, W.; Grabowska, E.; Zaleska-Medynska, A.; Łuczak, J. Fabrication and photoactivity of ionic liquid–TiO₂ structures for efficient visible-light-induced photocatalytic decomposition of organic pollutants in aqueous phase. *Beilstein J. Nanotechnol.* **2018**, *9*, 580–590. [[CrossRef](#)] [[PubMed](#)]
25. Han, C.-C.; Ho, S.-Y.; Lin, Y.-P.; Lai, Y.-C.; Liang, W.-C.; Chen-Yang, Y.-W. Effect of π – π stacking of water miscible ionic liquid template with different cation chain length and content on morphology of mesoporous TiO₂ prepared via sol–gel method and the applications. *Microporous Mesoporous Mater.* **2010**, *131*, 217–223. [[CrossRef](#)]
26. Chen, Y.; Li, W.; Wang, J.; Gan, Y.; Liu, L.; Ju, M. Microwave-assisted ionic liquid synthesis of Ti³⁺ self-doped TiO₂ hollow nanocrystals with enhanced visible-light photoactivity. *Appl. Catal. B Environ.* **2016**, *191*, 94–105. [[CrossRef](#)]
27. Łuczak, J.; Paszkiewicz-Gawron, M.; Długocka, M.; Lisowski, W.; Grabowska, E.; Makurat, S.; Rak, J.; Zaleska-Medynska, A. Visible light photocatalytic activity of ionic liquid-TiO₂ spheres: Effect of the ionic liquid's anion structure. *ChemCatChem* **2017**, *9*, 4377–4388. [[CrossRef](#)]
28. Kim, S.; Ko, K.C.; Lee, J.Y.; Illas, F. Single oxygen vacancies of (TiO₂)₃₅ as a prototype reduced nanoparticle: Implication for photocatalytic activity. *Phys. Chem. Chem. Phys.* **2016**, *18*, 23755–23762. [[CrossRef](#)] [[PubMed](#)]
29. Jiang, Y.; Zhu, Y.J.; Cheng, G.F. Synthesis of Bi₂Se₃ Nanosheets by Microwave Heating Using an Ionic Liquid. *Cryst. Growth Des.* **2006**, *6*, 2174–2176. [[CrossRef](#)]
30. Kaper, H.; Sallard, S.B.; Djerdj, I.; Antonietti, M.; Smarsly, B.M. Toward a Low-Temperature Sol–Gel Synthesis of TiO₂(B) Using Mixtures of Surfactants and Ionic Liquids. *Chem. Mater.* **2010**, *22*, 3502–3510. [[CrossRef](#)]
31. Verma, Y.L.; Tripathi, A.K.; Singh, V.K.; Balo, L.; Gupta, H.; Singh, S.K.; Singh, R.K. Preparation and properties of titania based ionogels synthesized using ionic liquid 1-ethyl-3-methyl imidazolium thiocyanate. *Mater. Sci. Eng. B* **2017**, *220*, 37–43. [[CrossRef](#)]
32. Jing, L.; Wang, M.; Li, X.; Xiao, R.; Zhao, Y.; Zhang, Y.; Yan, Y.-M.; Wu, Q.; Sun, K. Covalently functionalized TiO₂ with ionic liquid: A high-performance catalyst for photoelectrochemical water oxidation. *Appl. Catal. B Environ.* **2015**, *166*, 270–276. [[CrossRef](#)]
33. Ravishankar, T.N.; Nagaraju, G.; Dupont, J. Photocatalytic activity of Li-doped TiO₂ nanoparticles: Synthesis via ionic liquid-assisted hydrothermal route. *Mater. Res. Bull.* **2016**, *78*, 103–111. [[CrossRef](#)]
34. Liu, H.; Liang, Y.; Hu, H.; Wang, M. Hydrothermal synthesis of mesostructured nanocrystalline TiO₂ in an ionic liquid–water mixture and its photocatalytic performance. *Solid State Sci.* **2009**, *11*, 1655–1660. [[CrossRef](#)]
35. Shahi, S.K.; Kaur, N.; Singh, V. Fabrication of phase and morphology controlled pure rutile and rutile/anatase TiO₂ nanostructures in functional ionic liquid/water. *Appl. Surf. Sci.* **2016**, *360*, 953–960. [[CrossRef](#)]
36. Yan, X.; Ohno, T.; Nishijima, K.; Abe, R.; Ohtani, B. Is methylene blue an appropriate substrate for a photocatalytic activity test? A study with visible-light responsive Titania. *Chem. Phys. Lett.* **2006**, *429*, 606–610. [[CrossRef](#)]
37. Ohtani, B. Photocatalysis A to Z—What we know and what we do not know in a scientific sense. *J. Photochem. Photobiol. C Photochem. Rev.* **2010**, *11*, 157–178. [[CrossRef](#)]
38. Li, F.-T.; Wang, X.-J.; Zhao, Y.; Liu, J.-X.; Hao, Y.-J.; Liu, R.-H.; Zhao, D.-S. Ionic-liquid-assisted synthesis of high-visible-light-activated N–B–F-tri-doped mesoporous TiO₂ via a microwave route. *Appl. Catal. B Environ.* **2014**, *144*, 442–453. [[CrossRef](#)]
39. Mirhoseini, F.; Salabat, A. Ionic liquid based microemulsion method for the fabrication of poly (methyl methacrylate)–TiO₂ nanocomposite as a highly efficient visible light photocatalyst. *RSC Adv.* **2015**, *5*, 12536–12545. [[CrossRef](#)]
40. Raj, K.J.A.; Viswanathan, B. Effect of surface area, pore volume and particle size of P25 titania of the phase transformation of anatase to rutile. *Indian J. Chem.* **2009**, *48A*, 1378–1382.

41. Djerdj, I.; Tonejc, A.M. Structural investigations of nanocrystalline TiO₂ samples. *J. Alloys Compd.* **2006**, *413*, 159–174. [[CrossRef](#)]
42. Naumkin, A.V.; Kraut-Vass, A.; Gaarenstroom, S.W.; Powell, C.J. NIST X-ray Photoelectron Spectroscopy Database, NIST Standard Reference Database 20, Version 4.1. 2012. Available online: <http://srdata.nist.gov/xps/> (accessed on 25 March 2013).
43. Hu, X.; Zhang, T.; Jin, Z.; Zhang, J.; Xu, W.; Yan, J.; Zhang, J.; Zhang, L.; Wu, Y. Fabrication of carbon-modified TiO₂ nanotube arrays and their photocatalytic activity. *Mater. Lett.* **2008**, *62*, 4579–4581. [[CrossRef](#)]
44. Janus, M.; Inagaki, M.; Tryba, B.; Toyoda, M.; Morawski, A.W. Carbon-modified TiO₂ photocatalyst by ethanol carbonisation. *Appl. Catal. B Environ.* **2006**, *63*, 272–276. [[CrossRef](#)]
45. Kusiak-Nejman, E.; Janus, M.; Grzmil, B.; Morawski, A.W. Methylene Blue decomposition under visible light irradiation in the presence of carbon-modified TiO₂ photocatalysts. *J. Photochem. Photobiol. A Chem.* **2011**, *226*, 68–72. [[CrossRef](#)]
46. Li, Y.; Wang, Y.; Kong, J.; Jia, H.; Wang, Z. Synthesis and characterization of carbon modified TiO₂ nanotube and photocatalytic activity on methylene blue under sunlight. *Appl. Surf. Sci.* **2015**, *344*, 176–180. [[CrossRef](#)]
47. Wei, X.-N.; Wang, H.-L.; Wang, X.-K.; Jiang, W.-F. Facile synthesis of tunable carbon modified mesoporous TiO₂ for visible light photocatalytic application. *Appl. Surf. Sci.* **2017**, *412*, 357–365. [[CrossRef](#)]
48. Qi, H.-P.; Liu, Y.-Z.; Chang, L.; Wang, H.-L. In-situ one-pot hydrothermal synthesis of carbon-TiO₂ nanocomposites and their photocatalytic applications. *J. Environ. Chem. Eng.* **2017**, *5*, 6114–6121. [[CrossRef](#)]
49. Wu, D.; Long, M.; Cai, W.; Chen, C.; Wu, Y. Low temperature hydrothermal synthesis of N-doped TiO₂ photocatalyst with high visible-light activity. *J. Alloys Compd.* **2010**, *502*, 289–294. [[CrossRef](#)]
50. Dolat, D.; Quici, N.; Kusiak-Nejman, E.; Morawski, A.W.; Puma, G.L. One-step, hydrothermal synthesis of nitrogen, carbon co-doped titanium dioxide (N, CTiO₂) photocatalysts. Effect of alcohol degree and chain length as carbon dopant precursors on photocatalytic activity and catalyst deactivation. *Appl. Catal. B Environ.* **2012**, *115*, 81–89. [[CrossRef](#)]
51. Peng, F.; Cai, L.; Huang, L.; Yu, H.; Wang, H. Preparation of nitrogen-doped titanium dioxide with visible-light photocatalytic activity using a facile hydrothermal method. *J. Phys. Chem. Solids* **2008**, *69*, 1657–1664. [[CrossRef](#)]



© 2018 by the authors. Licensee MDPI, Basel, Switzerland. This article is an open access article distributed under the terms and conditions of the Creative Commons Attribution (CC BY) license (<http://creativecommons.org/licenses/by/4.0/>).